

## Pressure ionization in dense plasmas

G. Chiu and A. Ng

*Department of Physics and Astronomy, University of British Columbia, Vancouver, British Columbia, Canada V6T 1Z1*

(Received 27 March 1998)

We present an atomic model for assessing pressure ionization in a dense, strongly coupled plasma. The model is constructed in the framework of collisional-radiative equilibrium and detailed-configuration accounting, in which the effect of pressure ionization is described by the shift and broadening of energy levels. Its noteworthy feature is the use of a screening length based on a modified treatment of incipient Rydberg states. Using this model, we have identified signatures suitable for testing predictions of ionization balances and excited state populations, as well as a new approach for measuring the opacity of an absorption line in a well-defined plasma state. [S1063-651X(98)15712-4]

PACS number(s): 52.25.Jm, 62.50.+p, 64.30.+t, 64.70.-p

### I. INTRODUCTION

At sufficiently low densities, ions in a plasma can be considered as isolated atoms with unperturbed bound states. As the density increases, screening effects due to neighboring electrons and ions begin to modify the energy levels of the bound states while degeneracy begins to raise the energy of the free electrons. The resulting change in the ionization potentials of bound states and level occupation numbers leads to the phenomenon of pressure ionization [1]. This is the dominant process that determines the ionic abundances and level populations in high-density matter. The underlying importance of pressure ionization is substantial. To produce an equation of state one needs to determine first the ionization balance before computing the electron pressure. In the calculation of transport coefficients such as conductivities, the cross sections are functions of electron density and hence ionization balance. Radiative opacities are governed by both ionic abundances and level populations. All of these are properties of fundamental interest in plasma physics and are crucial to the development of stellar models [2] as well as inertial confinement fusion.

In spite of its central significance, ionization physics is often discussed implicitly as a part of a theoretical model describing equations of state [3], transport coefficients [4,5], or radiative opacities [6,7]. This may stem from the difficulty that quantities characterizing ionization, such as average ionization, ionic abundances, and level populations cannot be readily measured in experiments. There is no published theoretical result on ionic abundances and level populations at above-solid densities. There is also no reported experiment to directly probe pressure ionization in such plasmas. The latter can be attributed to the difficulty in producing a plasma with a sufficiently high density but a relatively low temperature such that the density effect on ionization is not obscured by the effect of thermal excitation.

In this paper, we present an atomic model for assessing pressure ionization in a dense, strongly coupled plasma. The model is constructed in the framework of collisional-radiative equilibrium and detailed-configuration accounting, in which the effect of pressure ionization is described by the shift and broadening of energy levels. Its noteworthy feature is the use of a screening length based on a modified treat-

ment of incipient Rydberg states. The model allows for detailed calculations of ionic abundances and level populations. It also enables us to identify signatures suitable for testing predictions of ionization balances and excited state populations as well as an approach for measuring the opacity of an absorption line in a well-defined plasma state.

### II. MODEL DESCRIPTION

There are two general approaches for the calculation of ionic abundances and level populations. In the chemical picture, the plasma is considered as a system of electrons, ions, and other composite particles such as molecules or clusters. Interparticle interactions are calculated from assumed potentials. Both atomic and thermodynamic properties may be derived from free energy minimization. A well-known example is the Opacity Project (OP) used to obtain solar opacity data at relatively low densities [6]. In the physical picture the plasma consists of only electrons and nuclei. Composite particles arise naturally. The properties of the plasma can be obtained from activity expansions of the grand canonical ensemble. A noted example is OPAL [7], which is used extensively for calculating emission and absorption spectra of hot plasmas. The treatment is rigorous in the weakly coupled plasma limit but computationally intensive and current activity expansions are limited to two-body terms.

Here, we have constructed a chemical model of aluminum consisting of electrons and ions. Using detail-configuration accounting (DCA) in a collisional-radiative equilibrium (CRE) framework, the bound and free electron state populations are governed by rate equations. Pressure ionization is treated by accounting for the effects of charge screening and electron-electron interactions on the energy of atomic levels.

Our model treats all ionization stages of aluminum described by their ground states together with about 500 excited states and approximately 900 line transitions. Collisional excitation and ionization, radiative recombination, autoionization and dielectronic recombination, as well as all inverse processes are considered. Up-to-date, critical rate coefficients for collisional ionization [8], autoionization [9], excitation [10], radiative recombination [11], and dielectronic recombination [12] are used. Unperturbed energy levels and transition probabilities are adopted from OP [6] and

RATION [13]. Forbidden line transitions in  $\text{Al}^{3+}$  to  $\text{Al}^{8+}$  are also considered [14–19]. Modifications on ionization rates due to dense plasma effects are given by Prenzel, Bornath, and Schlages [20].

Pressure ionization is described by the shift and broadening of energy levels. With reference to the isolated atom, shifts in energy levels have been calculated by Rogers, Graboske, and Harwood [21] and Roussel and O’Connell [22] from solutions of the Schrodinger equation using a screened Coulomb potential. At moderate densities, the use of screened potentials has already been shown by an independent calculation using pair distributions to yield the correct number of energy levels [23]. The results of Rogers, Graboske, and Harwood and Roussel and O’Connell are tabulated in the form of  $\Delta E^{nl}$  (shift in the eigenenergy of the level with principal quantum number  $n$  and orbital quantum number  $l$ ) as a function of the Debye-Huckel screening length  $\lambda_{\text{DH}}$  and the shell radius  $r^{nl}$  evaluated for a net ionic charge. To render these applicable to dense, strongly coupled plasmas, we introduce a new description of screening effects using a screening length  $D_s$  based on the concept of incipient Rydberg states (IRS) and a shell radius  $R^{nl}$  governed by the screened charge [24]. The former was formulated originally by Ichimaru [25] to differentiate screening effects between free and Rydberg states of hydrogen. For our calculations, it is necessary to reformulate the treatment for the various  $nl$  levels of aluminum. The corresponding screened potential is represented by

$$\begin{aligned} V_{nl}(r) &= \{-Q^{nl}e^2/r\}\exp\{-r/D_s\} \\ &= \{-Q^{nl}e^2/r\}\{A_f \exp(-r/\lambda_f) + A_{\text{IRS}} \\ &\quad \times \exp(-r/\lambda_{\text{IRS}})\}, \end{aligned}$$

where  $Q^{nl}$  is the screened hydrogenic charge [1],  $e$  the electron charge,  $\lambda_f = \{\epsilon_f/6\pi e^2 n_f\}^{1/2}$  the screening length due to free electrons,  $\lambda_{\text{IRS}} = (a_0/2)\{(2 + R^{nl}/\lambda_f)^3/(8 + 12R^{nl}/\lambda_f)\}$  the screening length due to IRS electrons,  $\epsilon_f$  the Fermi energy,  $n_f$  the free electron density, and  $a_0$  the Bohr radius.  $A_f$  and  $A_{\text{IRS}}$  describe the relative weighting of the free and IRS electrons [25]. To partition the electrons, we have adopted the partition function of Perrot [26],

$$Y = 1/\{1 + \exp[\alpha(X^{nl} - 1)]\},$$

whereby the densities of the free and incipient Rydberg states are given, respectively, by  $n_f = Yn_e$ ,  $n_{\text{IRS}} = (1 - Y)n_e$  for a total electron density  $n_e$ . This partition function is preferred over that proposed originally by Ichimaru because it gives rise to a more abrupt transition from IRS to free electron states consistent with explicit solutions of the Schrödinger equation [27,28]. The partition parameter is  $X^{nl} = E^{nl}/E_{\text{kin}}$  where the unshifted energy of the level,  $E^{nl}$ , is taken from OP [6] and the kinetic energies  $E_{\text{kin}}$  from results of density-functional-theory calculations [29]. The free parameter  $\alpha$  is set to 3 from a best fit of our average ionization values to those derived from density-functional-theory calculations [30] at a temperature of 5 eV and densities between 0.5–2 times the solid. This calibration is based on the expectation that at low temperatures and high densities, the con-

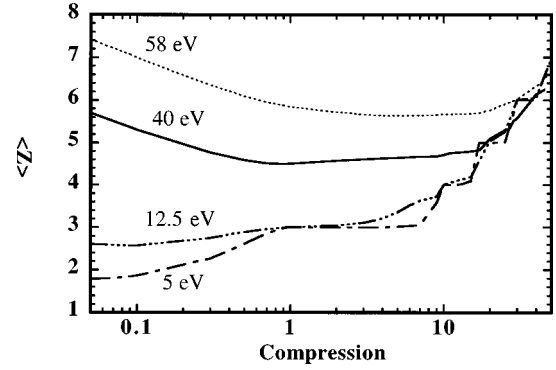


FIG. 1. Calculated  $\langle Z \rangle$  of Al as a function of compression at 5, 12.5, 40, and 58 eV.

densed matter model should be applicable. The results of our calculation is insensitive to  $\pm 20\%$  changes in the value of  $\alpha$ .

Finally, the broadening of energy levels is treated using the concept of degeneracy reduction or reduction in statistical weights [31]. Here, we have adopted the simple formula of Busquet [32], which yields  $\Pi^{nl} = 1 - (\Delta E^{nl}/E^{nl})$ , where  $\Pi^{nl}$  is the degeneracy reduction and  $\Delta E^{nl}$  is the shift in level energy.

### III. RESULTS OF CALCULATIONS

#### A. Comparison with other models and observation

As a general demonstration of the University of British Columbia atomic model (UBCAM), Fig. 1 shows a series of  $\langle Z \rangle$  isotherms plotted as a function of compression in aluminum. These illustrate that at any temperature, competition between three-body recombination and pressure ionization leads to a region of minimum ionization. The breadth of this minimum is largest at the lowest temperature. Since clusters are not treated in the model, current calculations are limited to densities above 1% of solid density. This, however, does not represent a serious constraint in the study of pressure ionization effects in dense plasmas.

Although more detailed information such as ionic abundances and level populations is obtained in our calculations, a direct comparison with other wide-range models such as the quotidian equation of state (QEOS) [3], Sesame [33], and density-functional-theory (DFT) [30] can only be made through  $\langle Z \rangle$ . As shown in Fig. 2, for aluminum at normal density the values of  $\langle Z \rangle$  derived from the different models

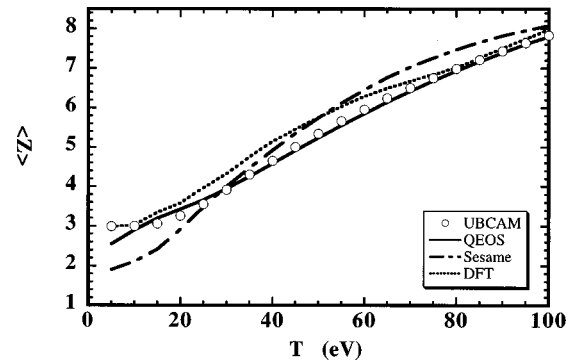


FIG. 2. Comparison of  $\langle Z \rangle$  of Al at normal density as a function of temperature derived from different models.

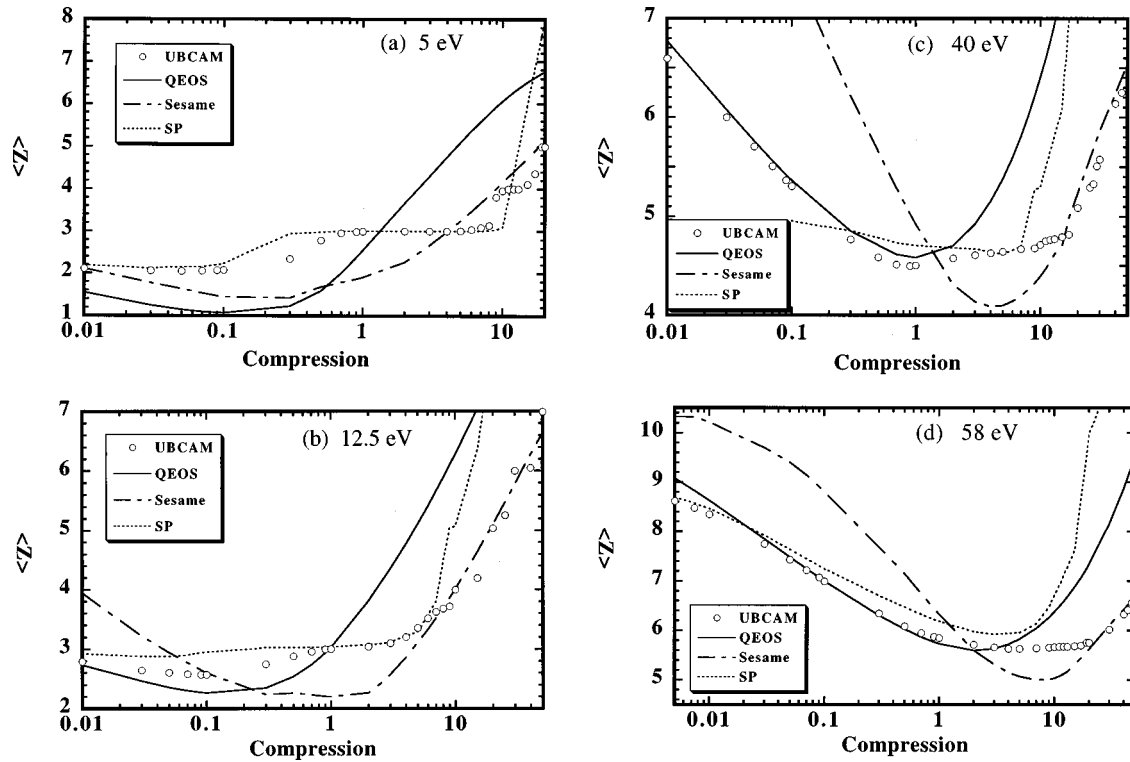


FIG. 3. Comparison of  $\langle Z \rangle$  of Al as a function of compression derived from different models at (a) 5, (b) 12.5, (c) 40, and (d) 58 eV.

differ by less than 0.6 except for Sesame at a temperature below 20 eV. For the calculation of plasma transport properties that depend only on  $\langle Z \rangle$ , this small discrepancy between models might be of minor concern. However, a small difference in  $\langle Z \rangle$  may correspond to vastly different ionic abundances that can impact significantly on radiative properties of the plasma.

Much greater discrepancies are revealed when comparisons are made at different densities, as illustrated in Fig. 3 which includes results from UBCAM, QEOS, and Sesame. This clearly underlines the need for experimental tests. It is interesting to note that at sufficiently high temperatures, our results appear to fall onto the low-density branch of QEOS and then cross over to the high-density branch of the Sesame model. Given the very different formalisms used in the different models, such behavior might be fortuitous.

Instead of evaluating the shifts of individual energy levels, pressure ionization can also be treated using the traditional method of continuum lowering, whereby the ionization potentials for all levels of the same ionization stage are reduced by the same amount as pressure increases. The concern with this latter approach is that it assumes identical screening effects on the inner as well as the outer shells. For comparison, we have performed calculations using our CRE-DCA model with the well-known continuum lowering formula of Stewart and Pyatt (SP) [34], in which the ionic charge is taken from a screened hydrogenic model [1]. The results are included in Fig. 3. These differ significantly from that obtained from level shift calculations only at high densities or high temperatures. A striking feature of the continuum lowering result is an abrupt increase in  $\langle Z \rangle$  near ten-fold compression. This is caused by the rapid, successive disappearance of the  $\text{Al}^{+3}$  through to the  $\text{Al}^{+6}$  stages as illustrated in Fig. 4.

One experimental test of our model calculations already exists for a strongly coupled plasma albeit at a low density. Using x-ray heating of a tamped layer, Perry *et al.* [35] measured the K-shell photoabsorption spectrum of an aluminum plasma at 58 eV and  $0.02 \text{ g/cm}^3$  (0.74% of solid density). Comparison with OPAL calculations yielded  $\langle Z \rangle$  of 8.1. As evident from Fig. 3(d), this appears to support predictions from QEOS and our model in which pressure ionization effects are described by either level shifts or continuum lowering. However, the observed  $\langle Z \rangle$  is significantly different from that given by the Sesame prediction.

The UBCAM treatment of ionization physics is based on the calculation of energy levels from solutions to the Schrödinger equation [21,22] in which the interaction potential is prescribed using a modified screening length and the calculation of level populations is governed by the self-consistent balance between energy levels and collisional-radiative rates as described by a set of rate equations. The appropriate incorporation of our model into a complete equation-of-state calculation is outside the scope of this work. However, it should be noted that the simple, *ad hoc* application of the  $\Delta E^{nl}$  term from the Stewart and Pyatt model to a Saha equation together with an ideal gas equation of state has been shown to lead to thermodynamic inconsistencies [36,37]. Such an approach can give rise to significant errors in parameters such as specific heats, electrical and thermal conductivities, and opacity.

## B. Ionization balance benchmarks

With the wide variations in theoretical predictions on ionization balance and the current lack of experimental data, it is crucial to identify benchmarks of atomic models based on

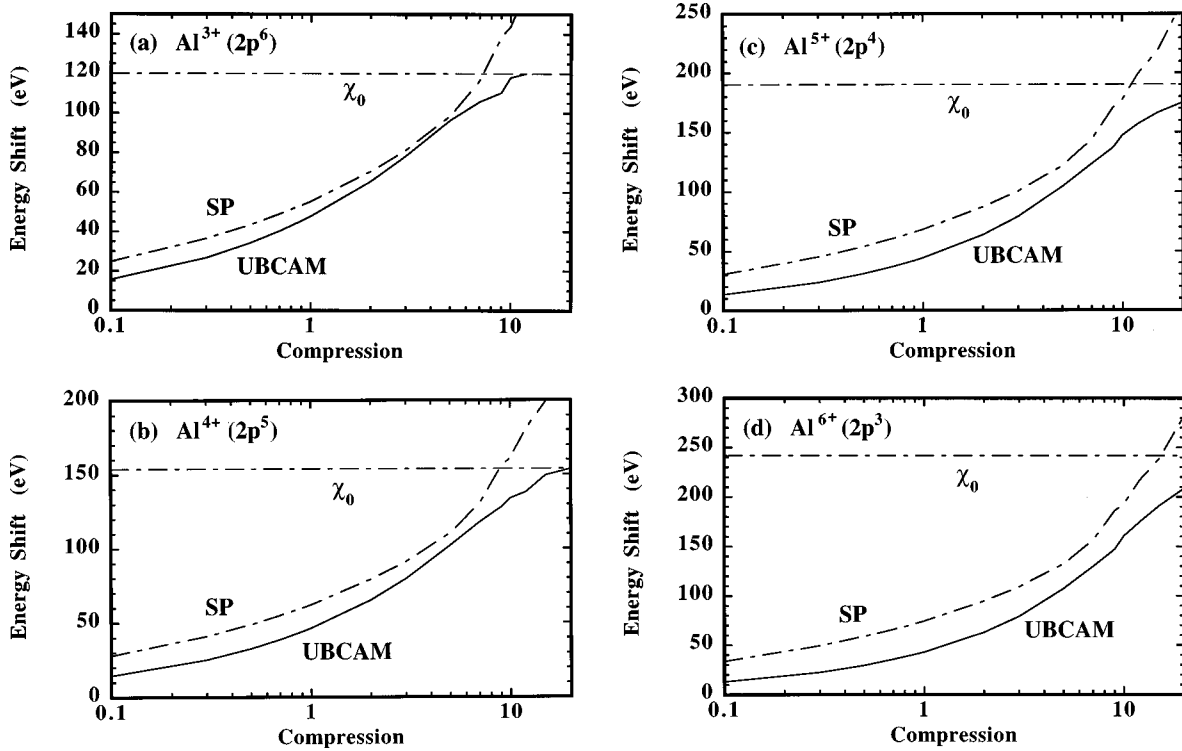


FIG. 4. Shifts of the ground-state energy levels of (a)  $\text{Al}^{3+}$ , (b)  $\text{Al}^{4+}$ , (c)  $\text{Al}^{5+}$ , and (d)  $\text{Al}^{6+}$  as a function of compression at 12.5 eV.  $\chi_0$  is the ionization potential.

unique, observable signatures that allow an unambiguous distinction between competing theories. Two examples are presented here.

First we consider the  $K\alpha$  photoabsorption spectroscopy of a dense and strongly coupled aluminum plasma at 2.5 times solid density and 12.5 eV. Such a plasma can be readily produced in the laboratory using a laser-driven shock wave. For example, hydrodynamic simulations [38] indicate that by irradiating a low- $Z$  ablator such as CH with a 532-nm laser pulse of nanosecond duration at a relatively modest irradiance of  $2 \times 10^{14}$  W/cm<sup>2</sup>, one can launch a 15-Mbar shock in CH. If this shock is allowed to propagate into a thin sample layer of aluminum sandwiched between pusher layers of silicon, impedance mismatch between CH and silicon would yield a 25-Mbar shock in the silicon while the ringing of the shock in aluminum between the silicon tampers would lead to the desired uniform and confined aluminum plasma. Silicon is both a close impedance-match to aluminum and a suitable window for x-ray absorption spectroscopy in the energy range of the aluminum  $K\alpha$  spectrum.

The ionic abundances of this aluminum plasma calculated from our atomic model are 93.3%  $\text{Al}^{3+}$ , 6.69%  $\text{Al}^{4+}$ , and 0.005%  $\text{Al}^{5+}$ , with  $\langle Z \rangle = 3.08$ . To compute the corresponding  $K\alpha$  absorption lines, we use oscillator strengths derived from dense plasma estimates [39] and linewidths due to electron collisional broadening using impact approximation [40]. The result for such an aluminum plasma with an areal mass density of  $6.75 \times 10^{-4}$  g/cm<sup>2</sup> is presented in Fig. 5. The thickness of the plasma is chosen to facilitate diagnostic access. Essentially the same result is obtained from calculations using continuum lowering to describe pressure ionization. On the other hand, level shift calculations using the partition function of Ichimaru [25] have yielded ionic abun-

dances of 33.4%  $\text{Al}^{4+}$  and 3.0%  $\text{Al}^{5+}$  with  $\langle Z \rangle = 3.4$ . This leads to nearly saturated absorption for the  $\text{Al}^{4+}$   $K\alpha$  line plus the appearance of an  $\text{Al}^{5+}$   $K\alpha$  absorption line as illustrated in Fig. 5. Accordingly, measurements of the  $K\alpha$  absorption line spectrum would readily test the suitability of the different partition functions.

For the plasma parameters described in the present example, QEOS yields  $\langle Z \rangle = 4.1$ . Although an absorption spectrum cannot be calculated without details of ionic abundances, such a  $\langle Z \rangle$  is likely to lead to substantial populations of  $\text{Al}^{4+}$  and  $\text{Al}^{5+}$  ions and the appearance of an even stronger  $\text{Al}^{5+}$   $K\alpha$  absorption line than in the case of  $\langle Z \rangle = 3.4$  described above. On the other hand, Sesame data suggest a  $\langle Z \rangle$  of 2.4. This should result in a much lower population of

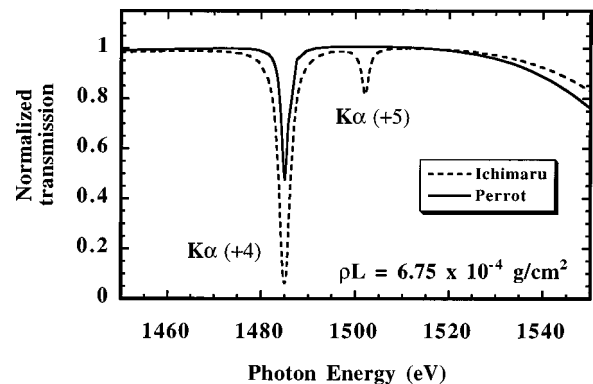


FIG. 5. Predicted  $\text{Al}^{4+}$   $K\alpha$  absorption line spectra from calculations using level shift or continuum lowering with Perrot's partition function, and from that using level shift with Ichimaru's partition function for an Al plasma at 12.5 eV and  $6.75$  g/cm<sup>3</sup> with an areal mass density of  $6.75 \times 10^{-4}$  g/cm<sup>2</sup>.

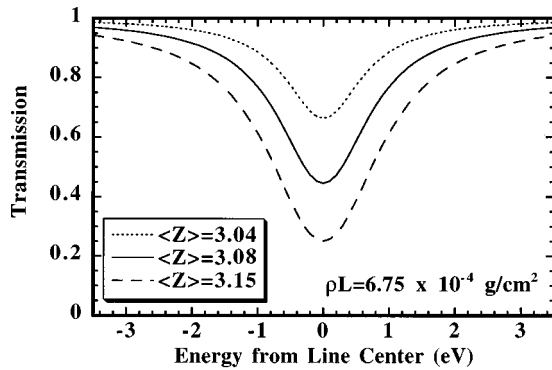


FIG. 6. Predicted  $\text{Al}^{+4}$   $K\alpha$  absorption line spectra for an Al plasma with an areal mass density of  $6.75 \times 10^{-4} \text{ g/cm}^2$  at 11.25 eV and  $6.08 \text{ g/cm}^3$  with  $\langle Z \rangle = 3.04$  (dotted line), 12.5 eV and  $6.75 \text{ g/cm}^3$  with  $\langle Z \rangle = 3.08$  (solid line), and 13.75 eV and  $7.43 \text{ g/cm}^3$  with  $\langle Z \rangle = 3.15$  (dashed line).

$\text{Al}^{+4}$  ions and hence a very weak  $\text{Al}^{+4}$   $K\alpha$  absorption line. These alternatives should be easily distinguishable in observations.

The sensitivity of the  $\text{Al}^{+4}$   $K\alpha$  absorption line as a  $\langle Z \rangle$  diagnostic is illustrated in Fig. 6. A variation of  $\pm 10\%$  in plasma density and temperature leads to readily measurable changes in the absorption line. On the other hand, even allowing for such a generous uncertainty in determining the plasma conditions, one can still set a tight limit on the value of  $\langle Z \rangle$  between 3.04 and 3.15. This is a particularly important aspect for using  $\langle Z \rangle$  in the benchmarking of ionization models. Figure 7 shows the implications of all three different models. The upper and the lower bounds of the iso- $\langle Z \rangle$  contours correspond to variations of  $\pm 10\%$  in both the plasma density and temperature. It is evident that whichever model is correct, the result will readily rule out the other two thus allowing the  $\langle Z \rangle$  benchmark to yield a unique differentiation of UBCAM, QEOS, and Sesame.

A similar benchmark can be obtained at even higher densities. For example, by propagating two colliding, 15-Mbar shock waves in an aluminum layer with an initial thickness of  $0.4 \mu\text{m}$  and embedded between silicon tampers, one can access an aluminum plasma at 5.4 times solid density and 18.2 eV [38]. The aluminum thickness is chosen to suit the diagnostic need. Our model again predicts a clear distinction in the results obtained from different partition functions (Fig. 8) and sets a limit on the value of  $\langle Z \rangle$  to within  $\pm 0.13$  for a  $\pm 10\%$  uncertainty in plasma density and temperature (Fig. 9). With corresponding theoretical values of  $\langle Z \rangle$  of 3.15 given by the Sesame model, 3.64 by UBCAM, and 5.26 by QEOS, the  $K\alpha$  absorption line spectrum will again be an excellent signature to differentiate these models as illustrated in Fig. 10.

### C. Persistence of excited states

To test the suitability of the level shift treatment versus that of continuum lowering, an obvious approach is to probe  $\langle Z \rangle$  of plasmas near 10 times solid density or above 40 eV as evident from Fig. 3. Such a high density or temperature might not be readily attainable in the laboratory, particularly for one-dimensional experiments that allow well-defined measurements of absorption spectra. Alternatively, one can

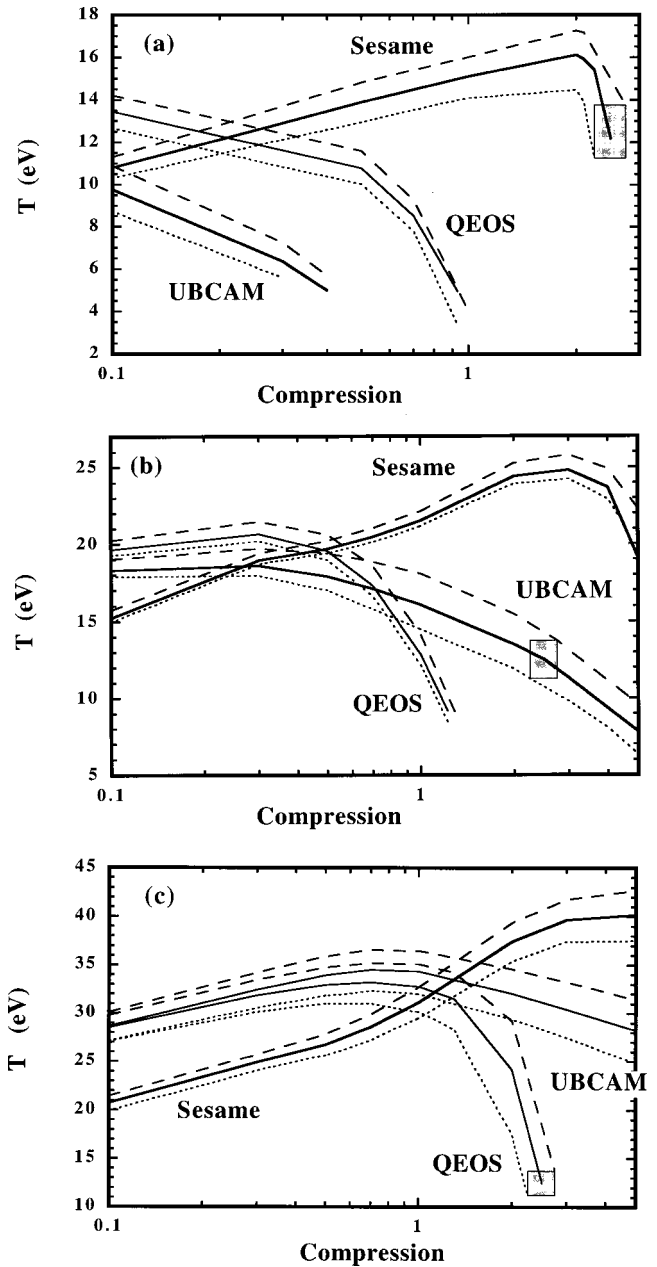


FIG. 7. (a) Contours for  $\langle Z \rangle$  of 2.34 (dotted line), 2.42 (solid line), and 2.50 (dashed line); (b) contours for  $\langle Z \rangle$  of 3.04 (dotted line), 3.08 (solid line), and 3.15 (dashed line); and (c) contours for  $\langle Z \rangle$  of 3.95 (dotted line), 4.11 (solid line), and 4.26 (dashed line) for the different models. The density-temperature range of the plasma considered is indicated by the shaded box.

seek an unique signature dictated by the details of level populations. Figure 11 shows the change in energy levels of the ground and excited states of the  $\text{Al}^{+3}$  ionization stage as a function of compression at 15 eV. Both our level shift calculation and the continuum lowering formula of Stewart and Pyatt show similar behavior for the ground state over a broad range of densities. On the other hand, at near-solid densities only the level shift calculation indicates the persistence of  $\text{Al}^{+3}$  excited states. With these,  $L$ -shell vacancies can be created that then allow for the appearance of an  $\text{Al}^{+3}$   $K\alpha$  absorption line as indicated in Fig. 12. For this

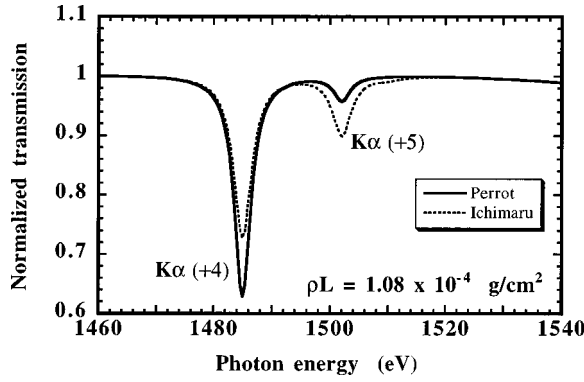


FIG. 8. Predicted  $Al^{+4}$   $K\alpha$  absorption line spectra from calculations using level shift treatment with Perrot's partition function, and from that with Ichimaru's partition function for an Al plasma at 18.2 eV and 14.6  $g/cm^3$ , with an areal mass density of  $1.08 \times 10^{-4} g/cm^2$ .

example, an aluminum plasma with an areal mass density of  $8.1 \times 10^{-5} g/cm^2$  is sufficient to provide the proper diagnostic access.

One possibility to produce an aluminum plasma at a near-solid density and modest temperature is shock compression of a layer of low-density aluminum foam embedded in a suitable tamper material. For example, a 4.5-Mbar shock in an aluminum foam of 15% normal density ( $0.4 g/cm^3$ ) will result in a plasma of 0.6 times normal density and a temperature of approximately 15 eV. Such a plasma might also be produced via x-ray heating of a aluminum layer sandwiched between low-Z tampers provided a sufficient flux of suitable x-rays is available.

**D. An approach to line opacity measurements**

Line opacity is of interest because in many plasmas, spectral lines are the dominant source of radiation transport [41]. Moreover, the analysis of spectral lines represents a well-defined means of probing level population and transition probability. An usual approach to line opacity measurement is the use of an inertially confined plasma produced by thermal, radiative or shock heating of a sample material sandwiched between tamper layers. For these plasmas, indepen-

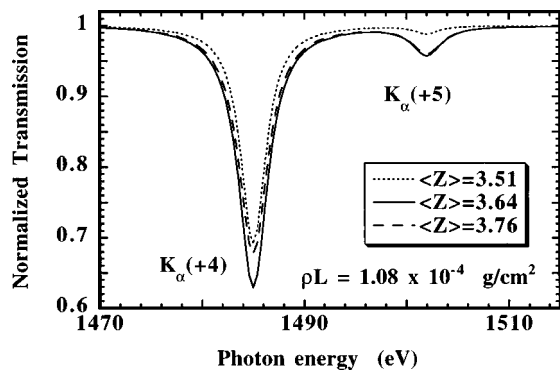


FIG. 9. Predicted  $Al^{+4}$  and  $Al^{+5}$   $K\alpha$  absorption line spectra for an Al plasma at 16.38 eV and 13.12  $g/cm^3$  with  $\langle Z \rangle = 3.51$  (dotted line), 18.2 eV and 14.58  $g/cm^3$  with  $\langle Z \rangle = 3.64$  (solid line), and 20.02 eV and 16.04  $g/cm^3$  with  $\langle Z \rangle = 3.76$  (dashed line). The areal mass density of the plasma is taken to be  $1.08 \times 10^{-4} g/cm^2$ .

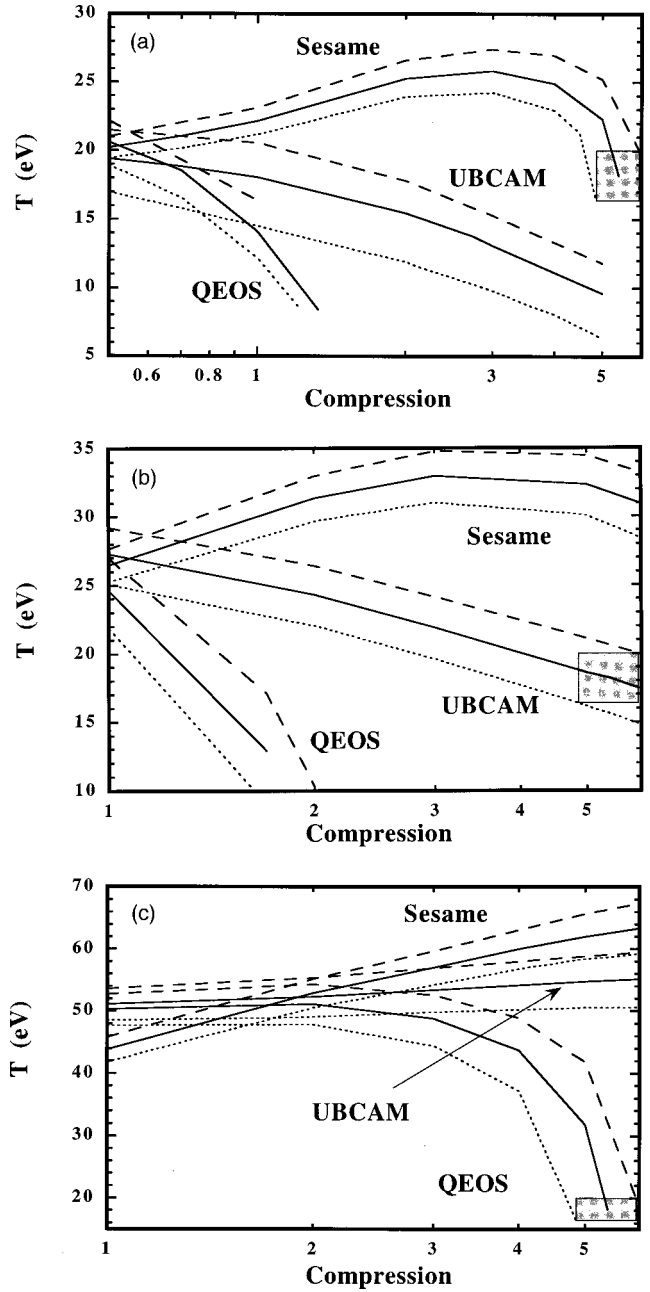


FIG. 10. (a) Contours for  $\langle Z \rangle$  of 3.04 (dotted line), 3.15 (solid line), and 3.26 (dashed line); (b) contours for  $\langle Z \rangle$  of 3.51 (dotted line), 3.64 (solid line), and 3.76 (dashed line); and (c) contours for  $\langle Z \rangle$  of 5.09 (dotted line), 5.26 (solid line), and 5.41 (dashed line) for the different models. The density-temperature range of the plasma considered is indicated by the shaded box.

dent determinations of plasma density and temperature are difficult. The plasma parameters are often derived only from hydrodynamic simulations.

A new approach to determine the opacity at the line center is to use a steady shock wave, measuring both the shock speed and the transmitted intensity of a backlighter source. As the shock propagates in the sample of interest, a plasma of uniform density and temperature is produced with a thickness that increases linearly with time. The resulting optical depth,  $\tau = \sigma \rho_o U_S t$ , would also increase linearly with time, where  $\sigma$  is the photoabsorption cross section in the compressed material,  $\rho_o$  the initial mass density of the sample,

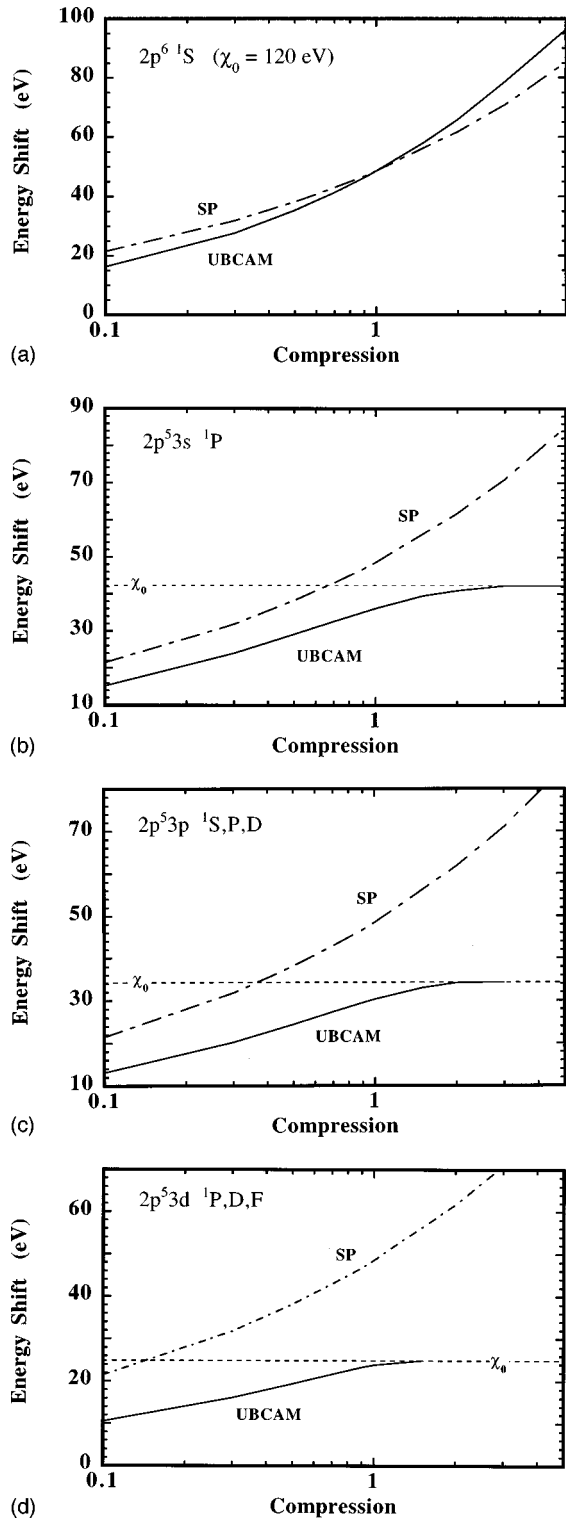


FIG. 11. Shifts of energy levels of the ground and excited states of  $\text{Al}^{+3}$  as a function of compression at 15 eV.  $\chi_0$  is the ionization potential.

$U_S$  the shock speed, and  $t$  the time of shock propagation. The transmitted intensity of a backlight source is  $I_T = I_o \exp(-\tau)$ , where  $I_o$  is the intensity of the source before entering the sample layer. The slope of  $\ln I_T$  plotted against  $t$  yields the product  $(-\sigma \rho_o U_S)$  and hence  $\sigma$  since  $U_S$  is measured. As the state of the shocked material lies along the principal Hugoniot, the observed shock speed can be used

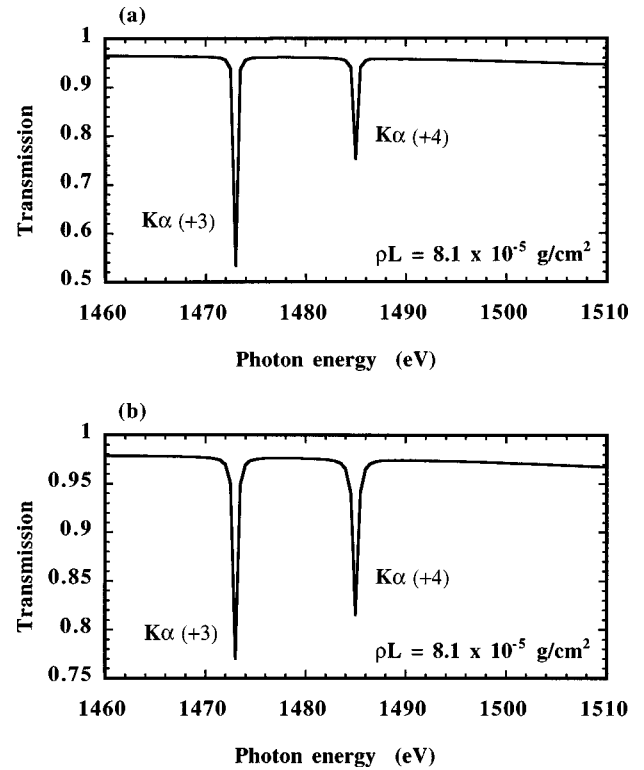


FIG. 12. Predicted  $\text{Al}^{+4}$   $K\alpha$  absorption line spectra from calculations using level shift or continuum lowering for an Al plasma with an areal mass density of  $8.1 \times 10^{-5} \text{ g/cm}^2$  at 15 eV and (a) 0.6 times solid density or (b) solid density.

with a known equation of state to yield the electron density  $n_e$  and temperature  $T_e$  of the plasma independent of the opacity diagnostic. Accordingly, the experiment yields  $\sigma(n_e, T_e)$ , the value of which can be used to test theoretical predictions of transition probabilities and level populations.

To illustrate this approach, we consider a steady shock wave of about 22 Mbar launched in a pusher layer of silicon before propagating into a sample layer of aluminum. Silicon is used to minimize the impedance mismatch and the difference in shock temperatures in the two materials. Furthermore, it is a suitable x-ray window for the desired spectroscopic measurement in aluminum. The shock pressure in aluminum will be 24 Mbar and the shock speed will be  $3.7 \times 10^6 \text{ cm/s}$ . This results in an aluminum plasma of  $3.1 \times$

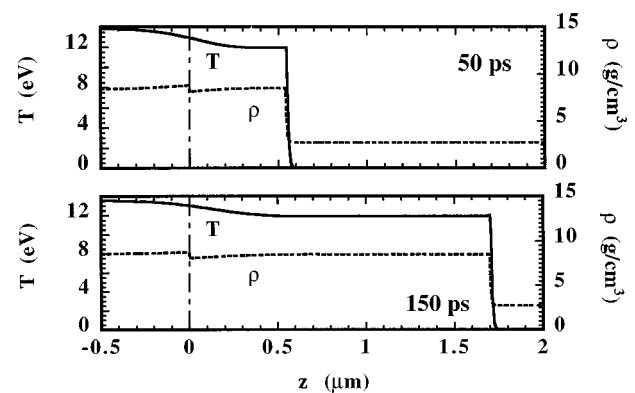


FIG. 13. Snapshots of temperature and mass density profiles in a 15-Mbar shock wave through a Si-Al sample.

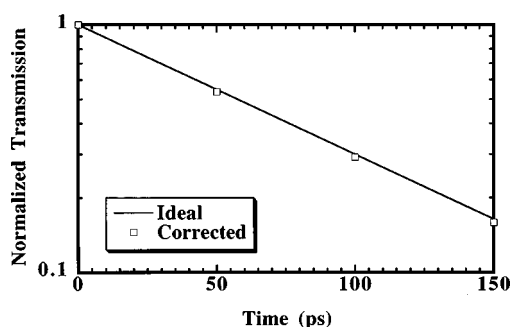


FIG. 14. Calculated transmitted intensity of the  $\text{Al}^{+4}$   $K\alpha$  absorption line as a function of time.

solid density and 12 eV. Figure 13 shows snapshots of the temperature and mass density profiles in the shock wave calculated from hydrodynamic simulations using a quotidian equation of state [3] and dense plasma conductivities [4]. The small gradients of temperature and density near the silicon-aluminum interface is the result of impedance mismatch. For the shocked aluminum, our model yields ionic abundances of 80.8%  $\text{Al}^{+3}$  and 19.2%  $\text{Al}^{+4}$  with a  $\langle Z \rangle$  of 3.20. This leads to a well-defined  $\text{Al}^{+4}$   $K\alpha$  absorption line similar to that presented in Fig. 5. The calculated transmitted intensities corresponding to this absorption line are presented in Fig. 14. The idealized results assumed uniform temperature and density in the shocked aluminum. As a simple estimate of thermal conduction effects, the “corrected” transmitted intensity is calculated by assuming that the nonuniform region near the silicon-aluminum interface is maintained at the averaged temperature across the gradient. Evidently, thermal conduction appears to have negligible

consequences. The 150 ps of shock propagation in the aluminum layer corresponds to a total optical depth of 2. This is a sufficiently long duration of observation for the picosecond temporal resolution typical of x-ray streak cameras.

#### IV. CONCLUSIONS

In conclusion, we have described an atomic model that allows detailed calculations of ionic abundance and level populations in strongly coupled plasmas over a wide range of temperatures and densities. The use of a CRE-DCA framework and eigenvalues for a screened hydrogenic system renders the model readily adaptable to describe other materials, giving the model a high degree of versatility and practicality. The critical aspect is the interpretation of screening length using a modified prescription of incipient Rydberg states. The choice of partition function and the use of hydrogenic screened charges are crucial only at high densities and low temperatures. From the results of our calculations, we have shown that  $K\alpha$  absorption spectroscopy can be used to obtain the experimental benchmark of ionization balance to differentiate our model from QEOS and Sesame. The treatment of pressure ionization from level shift calculations can be tested from evidence of  $\text{Al}^{+3}$   $K\alpha$  absorption line. A new approach to measuring the opacity of a  $K\alpha$  absorption line has also been illustrated.

#### ACKNOWLEDGMENT

This work was supported by the Natural Sciences and Engineering Research Council of Canada.

- 
- [1] R. M. More, *Adv. At. Mol. Phys.* **21**, 305 (1985).  
 [2] W. Huebner, in *Physics of the Sun*, edited P. Sturrock (Reidel, Dordrecht, 1986), Vol. 1, p. 33.  
 [3] R. M. More, K. H. Warren, D. A. Young, and G. B. Zimmerman, *Phys. Fluids* **31**, 3059 (1988).  
 [4] Y. T. Lee and R. M. More, *Phys. Fluids* **27**, 1273 (1984).  
 [5] F. Perrot and M. W. C. Dharma-wardana, *Phys. Rev. A* **36**, 238 (1989).  
 [6] D. G. Hummer and D. Mihalas, *Astrophys. J.* **331**, 794 (1988); D. Mihalas, W. Dappen, and D. G. Hummer, *ibid.* **331**, 815 (1988).  
 [7] F. Rogers, F. Swenson, and C. Iglesias, *Astrophys. J.* **456**, 901 (1996); F. Rogers and D. Young, *Phys. Rev. E* **56**, 5876 (1997).  
 [8] M. A. Lennon *et al.*, *J. Phys. Chem. Ref. Data* **17**, 1285 (1988).  
 [9] M. Arnaud and R. Rothenflug, *Astron. Astrophys., Suppl. Ser.* **60**, 425 (1985).  
 [10] L. Vriens and A. H. M. Smeets, *Phys. Rev. A* **22**, 940 (1980).  
 [11] L. C. Johnson, *Astrophys. J.* **174**, 227 (1972).  
 [12] D. Post *et al.*, *At. Data Nucl. Data Tables* **20**, 397 (1977).  
 [13] R. W. Lee, *J. Quant. Spectrosc. Radiat. Transf.* **32**, 91 (1984); R. W. Lee and J. Larsen, *ibid.* **56**, 535 (1996).  
 [14] A. Hibbert *et al.*, *At. Data Nucl. Data Tables* **53**, 23 (1993).  
 [15] B. Fawcett, *At. Data Nucl. Data Tables* **31**, 495 (1984).  
 [16] B. Fawcett, *At. Data Nucl. Data Tables* **22**, 473 (1978); **34**, 215 (1986).  
 [17] K. C. Cheng *et al.*, *At. Data Nucl. Data Tables* **24**, 111 (1979).  
 [18] H. Zhang and D. Sampson, *At. Data Nucl. Data Tables* **63**, 275 (1996); B. Fawcett, *ibid.* **37**, 367 (1987).  
 [19] H. Zhang and D. Sampson, *At. Data Nucl. Data Tables* **56**, 41 (1994).  
 [20] R. Prenzel, Th. Bornath, and M. Schlanges, *Phys. Lett. A* **223**, 453 (1996).  
 [21] F. Rogers, H. Graboske, and D. Harwood, *Phys. Rev. A* **1**, 1577 (1970).  
 [22] K. Roussel and R. O’Connell, *Phys. Rev. A* **9**, 52 (1974).  
 [23] F. J. Rogers, *Astrophys. J.* **352**, 689 (1990).  
 [24] R. M. More, *J. Quant. Spectrosc. Radiat. Transf.* **27**, 345 (1982); R. Marchand, S. Caille, and Y. T. Lee, *ibid.* **43**, 149 (1990); F. Perrot, *Phys. Scr.* **39**, 332 (1989).  
 [25] S. Ichimaru, *Rev. Mod. Phys.* **65**, 255 (1993); S. Ogata, H. Kitamura, and S. Ichimaru, in *Elementary Processes in Dense Plasmas*, edited by S. Ichimaru and S. Ogata (Addison-Wesley, New York, 1995), p. 145.  
 [26] F. Perrot, *Phys. Rev. A* **42**, 4871 (1990).  
 [27] D. Liberman and J. Albritton, *J. Quant. Spectrosc. Radiat. Transf.* **51**, 197 (1994).

- [28] K. LaGattuta, in *Proceedings of the 13th International Conference on Laser Interaction and Related Phenomena*, edited by S. Nakai and G. Miley (AIP, Woodbury, New York, 1996), p. 146.
- [29] F. Perrot, *Phys. Rev. A* **20**, 586 (1979).
- [30] F. Perrot and M. W. C. Dharma-wardana, *Phys. Rev. E* **52**, 5352 (1995).
- [31] G. Zimmerman and R. M. More, *J. Quant. Spectrosc. Radiat. Transf.* **23**, 517 (1980).
- [32] M. Busquet, *J. Quant. Spectrosc. Radiat. Transf.* **43**, 91 (1990).
- [33] Sesame Data Table, Los Alamos National Laboratory, Material Number 23715.
- [34] J. C. Stewart and K. D. Pyatt, *Astrophys. J.* **144**, 1203 (1966).
- [35] T. Perry *et al.*, *Phys. Rev. Lett.* **67**, 3784 (1991).
- [36] M. A. Sweeney, *Astrophys. J.* **220**, 335 (1978).
- [37] G. Fontaine, H. M. Van Horn, K.-H. Bohm and T. C. Grenfell, *Astrophys. J.* **193**, 205 (1974).
- [38] P. Celliers, Ph.D. thesis, University of British Columbia, 1987.
- [39] R. M. More, in *Physics of Laser Plasma*, edited by A. Rubenchik and S. Witkowski, *Handbook of Plasma Physics* Vol. 3 (North-Holland, Amsterdam, 1991).
- [40] H. Griem, *Phys. Rev.* **165**, 258 (1968).
- [41] J. Aprueze *et al.*, *Phys. Rev. Lett.* **79**, 3190 (1997).